*Journal of Applied Pharmaceutical Research*
*Volume 13 Issue 5, Year of Publication 2025, Page 114 – 133*
*DOI: https://doi.org/10.69857/joapr.v13i5.1356*

Check for updates

**Research Article**

***JOURNAL OF APPLIED PHARMACEUTICAL RESEARCH*** | ***JOAPR***
***www.japtronline.com*** ***ISSN: 2348 – 0335***

# *FORMULATION AND OPTIMIZATION OF METFORMIN-BERBERINE LOADED SOLID LIPID NANOPARTICLES FOR THEIR NEUROPROTECTIVE EFFECTS IN THE BRAIN*

Ravina Yadav[1], Ruchi Jakhmola Mani[1], Arun K. Sharma[2], Ashish Kumar[2], Deepshikha Pande Katare[1]*

***Article Information***
Received: 2nd June 2025
Revised: 25th August 2025
Accepted: 29th September 2025
Published: 31st October 2025

**Keywords**
*Type 2 Diabetes, Solid lipid Nanoparticles, Box Behnken, Optimization, Oxidative stress*

***ABSTRACT***

**Background:** The increasing prevalence of Type 2 Diabetes Mellitus (T2DM) is associated with a heightened risk of developing Alzheimer's Disease (AD), highlighting the need for effective therapeutic strategies that address the shared pathophysiological mechanisms in both conditions. **Methodology:** The Metformin-Berberine loaded solid lipid particles (MBSLNs) were prepared by dispersion of different concentrations of stearic acid, polysorbate 80, poloxamer 407, sesame oil, metformin, and berberine. Factor screening studies have been done to identify the influential components. An optimization study was then conducted using a three-factor Box-Behnken design with Design-Expert software. In-Vivo studies confirmed the neuroprotective role of SLNs. **Results:** The optimized concentrations of the variable factors were determined using the overlay plot generated by the software, resulting in stearic acid (4.84%), polysorbate 80 (1.50%), Poloxamer 407 (1%), and sesame oil (0.31%). The responses, particle size (10–200 nm), zeta potential (> ±30 mV), and polydispersity index (PDI) (0–1) were achieved within the desired range. **Discussion:** The closeness in experimental and predicted values confirms the reliability of the optimization technique. The optimized formulation exhibits a significant reduction in oxidative stress, and decreased glucose levels were observed when compared to the control, indicating a neuroprotective effect of the formulation. **Conclusion:** The optimized MBSLNs were affected by the independent parameters examined, including stearic acid, polysorbate 80, Poloxamer 407, and sesame oil concentrations, with significant effects on particle size, zeta potential, and size distribution. The utilization of MBSLNs has emerged as a remarkably effective strategy for enhancing the biological activity of Metformin and berberine in treating T2DM-induced AD.

## *INTRODUCTION*

Type 2 Diabetes Mellitus (T2DM) and Alzheimer's Disease (AD) are two of the most rampant and complex chronic conditions that have significant impacts on global health. While they have traditionally been viewed as separate diseases affecting different organ systems (metabolic and neurological),

[1]*Proteomics and Translational Research Lab, Centre for Medical Biotechnology, Amity Institute of Biotechnology, Amity University, Noida. India 201301*
[2]*Department of Pharmacology, Amity Institute of Pharmacy, Amity University, Gurugram, Haryana, India 122413*

***For Correspondence:*** **drdeepshikha26@outlook.com**

emerging evidence suggests a close link between them. Specifically, research has shed light on the concept of T2DM-induced AD, highlighting the significant role T2DM plays as a risk factor for the development and progression of AD [1]. T2DM is characterized by insulin resistance, impaired glucose metabolism, and chronically elevated blood glucose levels [2]. These metabolic abnormalities not only affect peripheral tissues but also have detrimental effects on the brain. Conversely, Alzheimer's disease is a neurological disorder that worsens with time and is marked by a build-up of neurofibrillary tangles (NFT) and beta-amyloid plaques in the brain, leading to cognitive decline and memory impairment [3]. According to recent research, people with T2DM are more likely to acquire AD when compared to those without diabetes. In fact, some researchers have proposed the concept of "Type 3 diabetes," referring to AD as a form of brain-specific diabetes resulting from insulin resistance and impaired glucose metabolism in the brain [4].

This concept underscores the idea that the pathological mechanisms underlying T2DM can extend to the brain and contribute to the development of Alzheimer's. Insulin resistance, which is a key feature of T2DM, has been implicated in the pathogenesis of AD [5]. Insulin plays essential roles in the brain, including regulating glucose metabolism, promoting neuronal survival, and facilitating synaptic plasticity [6]. However, in individuals with insulin resistance, the brain becomes less responsive to the effects of insulin, impairing glucose uptake and utilization in brain cells [7]. Consequently, the brain's energy metabolism is compromised, leading to neurodegenerative processes and cognitive decline characteristic of AD. Furthermore, chronic hyperglycemia, a hallmark of T2DM, can promote the formation of beta-amyloid plaques and neurofibrillary tangles, which are pathological hallmarks of AD. Advanced glycation end products (AGEs), inflammation, and hyperglycemia induce oxidative stress, all of which play an essential role in neurodegeneration and synaptic dysfunction [8]. These processes further accelerate the progression of AD pathology in individuals with T2DM.

It is essential to comprehend the interplay between T2DM and AD to develop efficient preventive and treatment plans. Researchers aim to reduce the risk of AD in people with T2DM by focusing on shared risk factors and addressing the underlying causes. Although a variety of medications are available to treat these medical conditions, none of them offer a permanent solution or cure, and they have numerous side effects. Additionally, the high expense of treatment disturbs the nation's medical healthcare system, necessitating the development of alternative medications to treat the disease and solve this worldwide issue. Due to its exceptional ability to lower plasma glucose levels, metformin has long been the preferred treatment for type 2 diabetes [9]. Metformin may have adverse consequences despite its numerous potential benefits [10]. These adverse effects of Metformin can be minimized by combining it with herbal formulations.

The discipline of therapeutics has seen a renaissance of interest in herbal medicine in recent years. The potential of herbal products to offer safe and effective treatment options for various health disorders makes them significant in the field of therapeutics [11]. Herbal substances, in contrast to synthetic medications, are considered holistic in nature, as they can work through a variety of processes and exhibit synergistic effects. One herbal substance that shows potential as a therapeutic agent in the treatment of T2DM-induced AD is berberine, an isoquinoline alkaloid that has a variety of pharmacological properties [12]. With numerous health benefits, including glycemic control, antioxidant effects, anti-inflammatory activity, amyloid-beta regulation, and neuroprotection [13], berberine is a viable option for addressing the complex interactions between AD and T2DM. Since oxidative stress is a common feature of both T2DM and AD, Berberine's antioxidant qualities are especially pertinent in this context. Despite having different structures, berberine and metformin share many characteristics in their modes of action, and both may be very effective medications for the treatment of AD and type 2 diabetes [14,15]. Berberine, on the other hand, can alleviate metformin's intestinal intolerance. Better hypoglycemic effects could result from taking the two medications together [16,17].

Solid lipid nanocarriers (SLNs) are colloidal carriers designed for drug delivery applications, composed of excipients approved for use in medicines currently in human use. They offer various advantages, including improved biocompatibility both in vitro and in vivo, targeted drug delivery compared to conventional methods, and a favorable safety profile with controlled release [18]. Understanding the link between a control variable and a quality variable is essential to produce the optimal formulation for the manufacture of Metformin-Berberine Solid lipid

Nanoparticle (MBSLNs) with desired particle size, zeta potential, and PDI. Modifying one variable at a time while keeping all others constant is the traditional approach we use. This method requires us to check for all potential combinations of formulation, which is otherwise time-consuming, costly & unfavorable to identify & fix unforeseen problems.

Our method utilizes the design of experiments (DOE) to gather vital data for understanding the relationship between the response and the factors [19]. To maximize the therapeutic efficacy of metformin and berberine, the optimization method is a crucial tool for obtaining high-quality MBSLNs, as characterized by their zeta potential, particle size, and size distribution. Important nanoparticle properties, including size, shape, and surface charge, must be carefully considered when designing drug delivery systems strategically, as improving these attributes can enhance targeted drug delivery to specific tissues. As such, continuous research into nanoparticle characteristics remains vital for enhancing future drug delivery systems.

The purpose of the study was to identify formulation factors that affect the characterization and therapeutic effects of MBSLNs by utilizing RSM. This study aims to optimize the concentration of MBSLN and polymer to produce neuroprotective effects in the brain, as well as to identify variables that may impact large-scale development or the scale-up process. MBSLNs were employed as a model drug for the research. Box-Behnken design (BBD) was used to measure responses such as zeta potential, PDI, and particle size.

## *MATERIALS AND METHODS*

### Materials

Nanoparticles containing metformin and berberine were synthesized. The ingredients used, including stearic acid, poloxamer 407, sesame oil, and polysorbate 80, were sourced from a central drug house located in New Delhi, India. The remaining chemicals utilized in the preparation were all of analytical grade.

### Preparation of MBSLNs

Solid Lipid Nanoparticles (SLNs) of Metformin and Berberine were prepared using the hot homogenization method [20], followed by ultrasonication. It includes the formation of a pre-emulsion of both drugs, surfactant, and water, at 60° C (aqueous phase) and a pre-emulsion of lipid and Sesame oil **(oil phase)**. The ingredients used in the formulation were stearic acid (Lipid), poloxamer 407 (stabilizer and surfactant), and sesame oil. Firstly, the hot aqueous phase was mixed with the oil phase dropwise via 22-gauge injections. Further, it was homogenized at 25,000 rpm for 10 minutes at a temperature of 4°C. The process continued with the emulsion being subjected to sonication using an ultrasonicator for a duration of 30 minutes. Subsequently, the mixture was left undisturbed at ambient temperature for 24 hours to facilitate hardening. Following this period, the mixture underwent centrifugation at a speed of 16,000 revolutions per minute (RPM), after which it was filtered and rinsed to yield the solid lipid nanoparticles. To conclude, the SLNs were air-dried at ambient temperature and preserved in a desiccator as documented in reference [21].

### Factor screening studies

A fractional factorial design with five factors and ten runs was employed to conduct factor screening studies, aiming to pinpoint the factors that have a significant impact on the properties of nanogels. The design matrix, presented in Table 1, enumerates the factors under investigation. These screening studies adhere to the “factor sparsity” principle, which involves selecting a subset of factors from a larger pool to identify the primary experimental variations that influence the drug product. Factors that were deemed responsible for notable variations were classified as influential or active, whereas the rest were categorized as less impactful or noise variables, as cited in reference [22]. A total of 24 formulations were crafted using the hot homogenization technique. These formulations underwent characterization, foregoing certain essential quality attributes. A polynomial equation was derived, and the influence of each factor on the response variable was assessed by examining its interactive effects. To quantitatively evaluate the impact of each independent variable on the formulation, both half-normal plots and Pareto charts were utilized.

### Optimization of MBSLNs

An optimization study for nanoparticle formulation was conducted using BBD [23] with the aid of Design-Expert software (Version 12) [24], aiming to achieve a formulation with targeted attributes. Based on initial studies, various parameters were chosen for further optimization. The independent variables consisted of stearic acid (F1), poloxamer 407 (F2), polysorbate 80 (F3), and sesame oil (F4). The optimization focused on

dependent variables, including particle size (Y1), zeta potential (Y2), and polydispersity index (PDI) (Y3), which were identified as key factors influencing these variables. A three-factor BBD with three levels was utilized to depict the response surface's characteristics during experimental runs, facilitating the identification of the optimal combination of experiments. The specific levels assigned to each independent variable are detailed in Table 1.

**Table 1: Level of each independent variable used in MBSLN**

| | Factor 1 | Factor 2 | Factor 3 | Factor 4 |
|---|---|---|---|---|
| **Run** | **A: Stearic Acid (g)** | **B: Polysorbate 80 (ml)** | **C: Poloxamer 407 (g)** | **D: Sesame oil (ml)** |
| **1** | 5 | 1.5 | 2 | 0.55 |
| **2** | 5 | 1 | 1.5 | 0.55 |
| **3** | 1 | 2 | 1.5 | 0.55 |
| **4** | 5 | 1.5 | 1 | 0.55 |
| **5** | 3 | 2 | 1.5 | 0.1 |
| **6** | 3 | 2 | 1 | 0.55 |
| **7** | 3 | 1 | 1 | 0.55 |
| **8** | 1 | 1.5 | 1.5 | 1 |
| **9** | 5 | 1.5 | 1.5 | 0.1 |
| **10** | 3 | 2 | 1.5 | 1 |
| **11** | 3 | 1.5 | 2 | 0.1 |
| **12** | 3 | 1 | 1.5 | 1 |
| **13** | 3 | 2 | 2 | 0.55 |
| **14** | 3 | 1.5 | 1 | 1 |
| **15** | 3 | 1.5 | 1 | 0.1 |
| **16** | 1 | 1 | 1.5 | 0.55 |
| **17** | 5 | 1.5 | 1.5 | 1 |
| **18** | 3 | 1.5 | 2 | 1 |
| **19** | 3 | 1 | 1.5 | 0.1 |
| **20** | 1 | 1.5 | 1 | 0.55 |
| **21** | 1 | 1.5 | 2 | 0.55 |
| **22** | 1 | 1.5 | 1.5 | 0.1 |
| **23** | 3 | 1 | 2 | 0.55 |
| **24** | 5 | 2 | 1.5 | 0.55 |

The study assessed the independent variables across three distinct levels: low (-1), baseline (0), and high (+1), encompassing 24 experimental runs, with 5 centered runs. To minimize the impact of uncontrolled factors, randomization was employed. The following equation is the statistical model that was fitted to the experimental data:

$$Y = \beta 0 + \beta 1A + \beta 2B + \beta 3C + \beta 4D + \beta 11A2 + \beta 22B2 + \beta 33C2 + \beta 44D2 + \beta 12AB + \beta 13AC + \beta 23BC + \beta 14AD + \beta 24BD + \beta 34CD$$

Where: "Y" depicts the response; "A", "B", "C" and "D" indicate the independent variables of Stearic acid, polysorbate 80, Poloxamer 407 and sesame oil conc, respectively The β11, β22, β33, and β44 represent the double-action coefficient for each variable i.e quadratic coefficients, β12, β13, β14, β23, β24, and β34 coefficients indicate interaction degree while β0 is a constant which means the intercept coefficient i.e center point regression coefficient in the equation above. An analysis of variance, p-value analysis, and regression coefficient evaluation were used to examine the regression model closely. Fisher's test was used to determine the validity of the second-order model, and the multiple coefficients of determination (R2) were used to evaluate the model's fit quality [25]. Based on response data, the software's point prediction algorithms were used to determine the best formulation. Following that, the formulation underwent additional assessments, including in vitro compatibility investigations, histological evaluations, biochemical evaluations, and statistical analysis.

## CHARACTERIZATION

### Particle size and zeta potential

The particle size and polydispersity index (PDI) of each formulation were assessed using a Zetasizer (Nano ZS, Malvern Instruments Ltd., UK) by the dynamic light scattering (DLS) technique. Before analysis, all samples have been diluted 100-fold with ultrapure water. Size measurements were conducted at a scattering angle of 173° utilizing the backscattering method. The same equipment was used to evaluate electrophoretic mobility for determining zeta potential values. All measurements were performed in triplicate to ensure precision.

### PDI

The PDI of each formulation was assessed using a Zetasizer (Nano ZS, Malvern Instruments Ltd., UK). Before analysis, all samples were diluted 100-fold with ultrapure water to minimize scattering effects. Size measurements were conducted at a fixed scattering angle of 173 ° at a temperature of 25 ± 0.1 °C. The software in the instrument calculated the PDI values using the cumulative analysis, which showed the breadth size of particles. All measurements were performed in triplicate to ensure precision.

### Entrapment Efficiency (EE)

The ultracentrifugation method was used to determine the entrapment efficiency of the formulations. Samples were spun

using a Microcentaur centrifuge for one hour at 13,000 rpm. After collecting the supernatant comprising unentrapped ciprofloxacin, high-performance liquid chromatography (HPLC) was used to measure the concentration of the free drug. The percentage entrapment efficiency (%EE) of the nanoparticle formulations was estimated using Equation (3):

$$\textbf{\textit{Entrapment efficency}}\ (\%) = \frac{\textbf{\textit{Total drug} - \textbf{\textit{Free drug}}}}{\textbf{\textit{Total drug}}}\ \textbf{\textit{X}}\ \mathbf{100}$$

*The measurements were performed in triplicate, and the mean values were calculated.*

**In vitro release study**

The in vitro drug release of the formulation was optimized via the dialysis bag method. Deionized water was used to immerse the dialysis tubing for 12 hours before use. A phosphate buffer was chosen as the release medium. Under continuous magnetic stirring at 100 rpm, a 2 mL aliquot of the formulation was placed into a dialysis bag, secured at both sides, and submerged in 25 mL of PBS maintained at 37 ± 1 °C. To maintain stable sink conditions, 1 mL of the release medium was removed and replaced with an equivalent volume of fresh PBS at predetermined intervals. The concentration of released medication was determined using HPLC. Every experiment was conducted in triplicate, and the mean ± standard deviation is used to report the results.

**Mechanism and kinetics of release studies**

Four mathematical models—zero-order, first-order, Higuchi, and Korsmeyer–Peppas—were employed to analyze the in vitro drug release data and determine the release mechanism and kinetics. These models were fitted with the Excel add-in DDsolver version 1 to determine the cumulative percentage drug release at each time point. For the Korsmeyer–Peppas model, the release exponent (n) was employed for the most prevalent release mechanism (Fickian diffusion). The model that best represented the release profile was selected based on the most significant adjusted coefficient of determination ($R^2$_adj) and model selection criterion (MSC) values, together with the lowest Akaike information criterion (AIC).

**Animal studies**

The Institutional Animal Ethics Committee approved the experimental procedures involving animals in this study in accordance with the guidelines established by the CPCSEA, as mandated by the Government of India, New Delhi. Adult Wistar rats, each weighing between 240 and 290 grams, were obtained from the Amity Institute of Pharmacy's animal facility. Animals were housed in polypropylene cages (4 per cage) with corn cob bedding, under controlled conditions of temperature (22 ± 2 °C), relative humidity (55 ± 5%), and a 12-h light–dark cycle, with ad libitum access to standard chow and water.

Animal health and behavior were monitored daily by trained staff, and any signs of distress or illness were promptly addressed in consultation with the institutional veterinarian. Investigators conducting behavioral, biochemical, and histological assessments were blinded to group allocations until completion of data analysis. Throughout this period, the rats were nourished with a conventional diet formulated for the rodent animal model.

**Toxin Model Development and Treatment Design**

The current study considered a total number of 27 animals (either sex), body weight ranging 180-200gm were randomly allocated to experimental groups (3 groups, n= 9 animals) using a computer-generated randomization sequence to ensure unbiased group distribution including normal control (normal saline treated), drug control (toxin treated), and treatment group (toxin treated followed by administration of MBSLNs). The combination of toxins included D-Galactosamine (10 mg/kg body weight), ethanol (8% v/v, 355 mL/60 kg body weight), and D-Galactose (100 mg/kg body weight), which were administered according to a predefined strategy as reported in our previous study [26]. The induction of the disease model was completed in three steps. The first step involved administering an oral dose of D-Galactosamine (10 mg/kg body weight).

This was followed by an oral dose of ethanol (8% ethanol, 355 mL/60 kg body weight) in the second step, administered 2 days after the first step. In the third step, d-galactose (100 mg/kg body weight) was administered after a 33-day gap. This cycle of all three steps was repeated in the same manner after a gap of 2 consecutive days for 90 days. The animals were monitored for behavioral analysis, and eventually, they were sacrificed at regular intervals for biochemical analysis and histopathological studies. Humane endpoints included severe lethargy or the inability to access food or water. Animals meeting these criteria were humanely euthanized in accordance with CPCSEA/Institutional Animal Ethics Committee guidelines.

**BEHAVIORAL ASSESSMENT**

**Water Morris maze test (MWM)**

The Morris water maze (MWM) test was done to evaluate the memory and cognition of the subjects. The subjects had previously been trained on the platform in a particular tank quadrant. After disease development, the test was repeated, and data were collected regarding the time required to reach the platform area and the time spent in the chosen quadrant [27].

**Y-maze test**

The raised Y–Maze Test is an essential behavioral test for measuring the rat's compliance to explore a new location. The hippocampus, septum, forebrain, and cortex are the main brain regions that are tested. The three opaque plastic arms in the Y-shaped maze test are positioned 120 degrees apart, and the subject should display an ability to enter a less-recently visited arm. The number of arm entries and triads was counted to determine the percentage of alteration [28].

**Histological evaluation**

Adult Wistar rats were sacrificed, and their livers, intestines, and brains were immediately removed and stored for histological analysis in 10% formalin buffer. After the tissues were fixed in paraffin wax, the blocks were sectioned into 4-µm-thick slides. Eosin (E) and Hematoxylin (H) were used to stain the sections [29]. The photomicrographs were examined under an Olympus CKX41SF inverted microscope system.

**Biochemical measurements and evaluation of neurotransmitter levels**

***Determination of Catalase Activity***

The Catalase assay was performed according to the method described by [30] with slight modifications. The test mixture of 3 mL contained 1.99mL of phosphate buffer (0.05M, pH 7), 1mL of $H_2O_2$ (20 20mM), and 10 µL of the brain tissue sample. The activity was measured in terms of n moles $H_2O_2$ consumed/min/mg protein by recording absorbance at 240nm [31].

***Determination of ACHE activity***

The AChE activity was estimated by using the protocol of Ellman et al. [32]. For AChE activity measurement, the reaction volume of 1.56 mL included 1.3 mL sodium phosphate buffer, 0.05 mL DTNB, 10 µL ATC, and 0.2 mL supernatant. The absorbance was measured at 412 nm. The AChE activity was expressed as micromoles of ATC hydrolyzed/min/mg protein [33,34].

***Glucose estimation***

Glucose estimation was performed using the Glucose Oxidase–Peroxidase (GOD-POD) method in an endpoint mode by using an Autospan Glucose Kit [35]. The absorbance was measured at 505 nm. Glucose levels were expressed as mg/Dl.

***Determination of Lipid Peroxidation***

A lipid peroxidation assay was performed using the protocol of Wright et al. (1981)[36] with certain modifications. The test mixture consisted of 0.5 mL of the brain tissue sample, 0.5 mL of TBA (0.67%), and 0.5 mL of TCA (10%). The absorbance was recorded at 532nm.

***Statistical Analysis***

The data obtained from the study were presented as the Mean ± Standard Error of Mean (SEM). Statistical evaluations were conducted using Origin 9.0 software. The comparison between the baseline (control) group and the experimental (treated) group was carried out using a one-way ANOVA, followed by a Tukey test for post-hoc analysis. A p-value less than 0.0001 was deemed to indicate a statistically significant difference.

***RESULTS AND DISCUSSION***

**Model Assessment**

As described in Figure 1, stearic acid (A), poloxamer 407 (B), polysorbate 80 (C), and sesame oil (D) exert a significant positive effect on the response particle size, zeta potential, and PDI. Thus, they were selected as three key factors for the formulation of the nanocarriers.

**Optimization Studies in Systemic Framework**

The screening study aimed to find out which factors were essential and which ones were not. This way, the number of experiments could be reduced without losing accuracy in the results. The experimental data were collected by using BBD, a method that adjusts the essential factors to their optimal values, while keeping the less important factors constant [37]. The different levels of the variables and the outcomes of the trials based on BBD are explained. The effect of formulation factors (Table 2) on MRT, viscosity, wound healing, and swelling index was investigated through 24 experiments with 5 center points. The data from the experimental runs by BBD is shown. This study's response is modeled as a quadratic function of the independent variables, and the functions were approximated using a first-order polynomial equation.

$$y = \beta 0 + \beta 1X1 + \beta 2X2 + \beta 3X3 + \beta 4X4 + \beta 5X1X2 + \beta 6X1X3 + \beta 7X1X4 + \beta 8X2X3 + \beta 9X2X4 + \beta 10X3X4\ 2 \quad (2)$$

*Where: "β" is the coefficient, and "X" is the independent variable.*

The value of response y1 (particle size), y2 (zeta potential), and y3 (PDI) ranges from 38.2 to 1662, -45 to -10, 0.307 to 0.767. For the response, the ratios of the highest and lowest values are 43.5, -4.5, and 2.49, respectively. Power transformation is thus not necessary for the acquired values.

**Table 2**: **The combination of various factors used in the formulation of MBSLN and responses**

| | **Factor** 1 | **Factor 2** | **Factor 3** | **Factor 4** | **Response 1** | **Response 2** | **Response 3** |
|---|---|---|---|---|---|---|---|
| **Run** | A: Stearic Acid | B: Polysorbate 80 | C: Poloxamer 407 | D: Sesame oil | Particle Size | Zeta Potential | PDI |
| | **g** | **mL** | **g** | **mL** | **nm** | **mV** | **%** |
| **1** | 5 | 1.5 | 2 | 0.55 | 334 | -38.5 | 0.332 |
| **2** | 5 | 1 | 1.5 | 0.55 | 38.2 | -28.4 | 0.456 |
| **3** | 1 | 2 | 1.5 | 0.55 | 250.4 | -31.8 | 0.458 |
| **4** | 5 | 1.5 | 1 | 0.55 | 56.85 | -31.9 | 0.334 |
| **5** | 3 | 2 | 1.5 | 0.1 | 496.1 | -38.8 | 0.405 |
| **6** | 3 | 2 | 1 | 0.55 | 218 | -32.7 | 0.46 |
| **7** | 3 | 1 | 1 | 0.55 | 73.5 | -22.9 | 0.337 |
| **8** | 1 | 1.5 | 1.5 | 1 | 76 | -18.9 | 0.486 |
| **9** | 5 | 1.5 | 1.5 | 0.1 | 497 | -32.6 | 0.478 |
| **10** | 3 | 2 | 1.5 | 1 | 254.8 | -32.7 | 0.5 |
| **11** | 3 | 1.5 | 2 | 0.1 | 931.7 | -28.6 | 0.75 |
| **12** | 3 | 1 | 1.5 | 1 | 200.3 | -24.9 | 0.579 |
| **13** | 3 | 2 | 2 | 0.55 | 62.5 | -45.6 | 0.359 |
| **14** | 3 | 1.5 | 1 | 1 | 214.2 | -23.4 | 0.392 |
| **15** | 3 | 1.5 | 1 | 0.1 | 317.6 | -27.6 | 0.307 |
| **16** | 1 | 1 | 1.5 | 0.55 | 1662 | -10.5 | 0.4 |
| **17** | 5 | 1.5 | 1.5 | 1 | 497 | -32.9 | 0.571 |
| **18** | 3 | 1.5 | 2 | 1 | 224 | -29.3 | 0.366 |
| **19** | 3 | 1 | 1.5 | 0.1 | 845 | -25.9 | 0.765 |
| **20** | 1 | 1.5 | 1 | 0.55 | 344 | -16.7 | 0.737 |
| **21** | 1 | 1.5 | 2 | 0.55 | 270.8 | -26.7 | 0.324 |
| **22** | 1 | 1.5 | 1.5 | 0.1 | 265 | -23.8 | 0.392 |
| **23** | 3 | 1 | 2 | 0.55 | 786 | -22.1 | 0.767 |
| **24** | 5 | 2 | 1.5 | 0.55 | 439.3 | -51.2 | 0.487 |

**Table 3: Overview of Model Response Metrics**

| **Source** | **Std. Dev.** | **$R^2$** | **Adjusted $R^2$** | **Predicted $R^2$** | **PRESS** |
|---|---|---|---|---|---|
| **Linear** | **3.56** | **0.8665** | **0.8384** | **0.7869** | **383.36** |
| 2FI | 3.62 | 0.9052 | 0.8322 | 0.6768 | 581.54 |
| Quadratic | 3.35 | 0.9378 | 0.8569 | 0.6416 | 644.93 |
| **Source** | **Std. Dev.** | **$R^2$** | **Adjusted $R^2$** | **Predicted $R^2$** | **PRESS** |
| Linear | 341.70 | 0.2738 | 0.1209 | -0.1587 | 3.540E+06 |
| **2FI** | **282.43** | **0.6605** | **0.3994** | **-0.1570** | **3.534E+06** |
| Quadratic | 298.74 | 0.7078 | 0.3280 | -0.6828 | 5.141E+06 |
| **Source** | **Std. Dev.** | **$R^2$** | **Adjusted $R^2$** | **Predicted $R^2$** | **PRESS** |
| Linear | 0.1535 | 0.0964 | -0.0938 | -0.4417 | 0.7142 |
| **2FI** | **0.1414** | **0.4752** | **0.0715** | **-0.7887** | **0.8861** |
| Quadratic | 0.1503 | 0.5440 | -0.0488 | -1.6266 | 1.30 |

The model summary statistics, sequential model sum of squares, and lack of fit test were used for choosing the model for response analysis (Table 3). The quadratic model for response analysis is represented by a high R-squared value, a low standard deviation, and a reduced projected residual error sum of squares (PRESS) value. ANOVA assessed the significance and effect of each variable on another variable. The quadratic model was found to be adequate by the ANOVA (Table 4) (model Probe>F is less

than 0.05–0.0001), which helped to identify the components that influenced the response (y1–y3) of nanoparticle formulation. The ratio of Poloxamer 407 and polysorbate 80 was significant for particle size, while for zeta potential, stearic acid and polysorbate 80 were essential. Polysorbate 80 and Poloxamer 407 were significant factors in determining the PDI.

**Table 4: ANOVA response for the surface model of particle size, zeta potential, and PDI**

| **Particle size** | | | | | |
|---|---|---|---|---|---|
| **Source** | **Sum of Squares** | **df** | **Mean Square** | **F-value** | **p-value** |
| **Model** | 2.018E+06 | 10 | 2.018E+05 | 2.53 | 0.0598 |
| A-Stearic Acid | 84311.19 | 1 | 84311.19 | 1.06 | 0.3227 |
| B-Polysorbate 80 | 2.958E+05 | 1 | 2.958E+05 | 3.71 | 0.0763 |
| C-Poloxamer 407 | 1.598E+05 | 1 | 1.598E+05 | 2.00 | 0.1804 |
| D-Sesame oil | 2.964E+05 | 1 | 2.964E+05 | 3.72 | 0.0760 |
| AB | 8.215E+05 | 1 | 8.215E+05 | 10.30 | 0.0068 |
| AC | 30686.28 | 1 | 30686.28 | 0.3847 | 0.5458 |
| AD | 8930.25 | 1 | 8930.25 | 0.1120 | 0.7433 |
| BC | 1.884E+05 | 1 | 1.884E+05 | 2.36 | 0.1484 |
| BD | 40682.89 | 1 | 40682.89 | 0.5100 | 0.4878 |
| CD | 91294.62 | 1 | 91294.62 | 1.14 | 0.3042 |
| **Residual** | 1.037E+06 | 13 | 79769.06 | | |
| **Zeta potential** | | | | | |
| **Source** | **Sum of Squares** | **df** | **Mean Square** | | |
| **Model** | 1559.04 | 4 | 389.76 | | |
| A-Stearic Acid | 632.20 | 1 | 632.20 | | |
| B-Polysorbate 80 | 801.97 | 1 | 801.97 | | |
| C-Poloxamer 407 | 105.61 | 1 | 105.61 | | |
| D-Sesame oil | 19.25 | 1 | 19.25 | | |
| **Residual** | 240.26 | 19 | 12.65 | | |
| **Cor Total** | 1799.30 | 23 | | | |
| **PDI** | | | | | |
| **Source** | **Sum of Squares** | **df** | **Mean Square** | **F-value** | **p-value** |
| **Model** | 0.2354 | 10 | 0.0235 | 1.18 | 0.3840 |
| A-Stearic Acid | 0.0016 | 1 | 0.0016 | 0.0805 | 0.7811 |
| B-Polysorbate 80 | 0.0336 | 1 | 0.0336 | 1.68 | 0.2174 |
| C-Poloxamer 407 | 0.0091 | 1 | 0.0091 | 0.4565 | 0.5111 |
| D-Sesame oil | 0.0034 | 1 | 0.0034 | 0.1717 | 0.6854 |
| AB | 0.0002 | 1 | 0.0002 | 0.0091 | 0.9254 |
| AC | 0.0422 | 1 | 0.0422 | 2.11 | 0.1699 |
| AD | 2.500E-07 | 1 | 2.500E-07 | 0.0000 | 0.9972 |
| BC | 0.0705 | 1 | 0.0705 | 3.52 | 0.0831 |
| BD | 0.0197 | 1 | 0.0197 | 0.9870 | 0.3386 |
| CD | 0.0550 | 1 | 0.0550 | 2.75 | 0.1212 |
| **Residual** | 0.2600 | 13 | 0.0200 | | |
| **Cor Total** | 0.4954 | 23 | | | |

**Table 5: Values of the regression term for responses**

| **S. no** | **Terms** | **y1** | **y2** | **y3** |
|---|---|---|---|---|
| **1** | **$R^2$** | 0.6605 | 0.8665 | 0.4751 |
| **2** | **Adjusted $R^2$** | 0.3994 | 0.8384 | 0.07148 |
| **3** | **Predicted $R^2$** | -0.1570 | 0.7869 | 0.7887 |
| **4** | **Adequate precision** | 6.3822 | 19.0170 | 3.8784 |

The model's strong predictability of response was demonstrated by the table's "Pred R-squared" value, which was found to be in fair agreement with the "Adj R-squared" value (Table 5). The equations below present the final mathematical model for responses y1–y3, estimated using Design-Expert software.

$$\mathbf{y1\ (particle\ size)} = +389.76 - 83.82 * A - 156.99 * B + 115.40 * C - 157.18 * D + 453.18 * AB + 87.59 * AC + 47.25 * AD - 217.00 * BC + 100.85 * BD - 151.07 * CD \quad \text{(Eq. 1)}$$

$$\mathbf{y2\ (zeta\ potential)} = -29.10 - 7.26 * A - 8.17 * B - 2.97 * C + 1.27 * D \quad \text{(Eq. 2)}$$

$$\mathbf{y3\ (PDI)} = +0.4768 - 0.0116 * A - 0.0529 * B + 0.0276 * C - 0.0169 * D - 0.0067 * AB + 0.1027 * AC - 0.0002 * AD - 0.1328 * BC + 0.0702 * BD - 0.1172 * CD \quad \text{(Eq. 3)}$$

A positive sign implies a synergistic impact, whereas a negative sign indicates an antagonistic effect. For y1 (particle size), the negative coefficient of A, B, and D suggests a decrease in particle size with an increase in these factors. In contrast, the positive coefficient of C, AD, BD, and AC indicates an increase in particle size with an increase in these factors. AD, BD, and AC, in combination, exert a synergistic effect on particle size. At the same time, BC has an antagonistic impact on particle size when combined, meaning that particle size decreases when these factors are present in high combination. The negative coefficients of the A, B, and C factors for the y2 (zeta potential) response show that a high concentration of these factors results in a drop in zeta potential. The positive coefficient of factor D indicates that the zeta potential increases with an increase in concentration of factor D. In the case of response y3, the negative coefficient of factors A, B, and D indicates a decrease in PDI with high concentrations of factor A, B, and D. In contrast, the positive coefficient of the combination of AC and BD and C indicates an increase in PDI when these factors increase or are in high combination in the formulation. When the experimental and theoretical values were compared using the diagnostic case statistic reports table, a fair amount of agreement was observed [Table 6].

To determine the most essential elements, the perturbation graph was plotted. [Figure 1]. In contrast to the comparatively flat line, a steeper slope denotes a greater effect of the factor on the response. Compared to factors A, B, and D, factor C exhibits a high slope in the case of y1 response, i.e., particle size, suggesting a strong effect on the response y1 in comparison to other components. Regarding response y2, the fact that factor B has a steeper slope than factor A suggests that it has a greater impact on response y2 than factors A and C. The steep slopes of factor B and factor C in y3 indicate that they have a significant effect on response PDI. The zeta potential is a measurement of the net electric charge on the surface of a nanoparticle, which quantifies the charges present on it. The concentration of ions with opposing charges close to the nanoparticle surface screens out charges when the particle has a net surface charge. This charge depends on the concentration of stearic acid, polysorbate 80, poloxamer 407, and sesame oil. Stearic acid is a long-chain fatty acid that can interact with its surroundings because it has a carboxyl group at the head and a hydrophobic tail. The carboxyl group of stearic acid may deprotonate, depending on the pH of the medium, which gives the nanoparticles' surface a negative charge. Because of the increased electrostatic repulsion & decreased aggregation between the particles, this negative charge raises the zeta potential & contributes to the stability of the nanoparticles [38]. Nanoparticles with higher zeta potential typically exhibit stronger electrostatic repulsion, which contributes to their stability by reducing the likelihood of aggregation [39]. Higher concentrations of stearic acid can indeed contribute to a more negative zeta potential [40].

Increasing the concentration of Poloxamer 407 can decrease zeta potential, which can be attributed to the formation of a sterically stabilized adsorbed polymer layer. Polysorbate 80, also used as a surfactant, plays a role in determining the zeta potential. Increasing the concentration of Tween 80 or polysorbate 80 can decrease the zeta potential, whereas the concentration of sesame oil has a positive correlation with zeta potential; as its concentration increases, the zeta potential increases as well. Particle size affects the stability, drug release rate, biodistribution, cellular uptake, penetration, and biological performance of nanoparticles [41, 42]. The optimal particle size ranges from 5 to 200 nm, which is used in drug delivery systems to enhance retention and permeability [43]. The particle size of nanoparticles depends on the type of surfactants, concentration of lipids, and other stabilizers.

The lipid used here is stearic acid, which significantly influences the particle size and exhibits an inverse correlation with particle size. This means that an increased concentration of stearic acid can decrease the particle size. Particle size also decreases when the concentration of Poloxamer 407 increases. Increasing the Poloxamer 407 concentration provides more coverage on the nanoparticle surface, stabilizing the system through steric hindrance and preventing particle growth. Sesame oil and Polysorbate 80 exhibit a negative correlation with particle size, indicating an increase in particle size with lower concentrations of sesame oil and Polysorbate 80.

**Table 6: Actual and predicted values of responses y1-y3**

| S No | Actual value | | | Predicted value | | | Residual | | |
|---|---|---|---|---|---|---|---|---|---|
| | y1 | **y2** | **y3** | y1 | **y2** | **y3** | y1 | **y2** | **y3** |
| 1 | 334.00 | -38.50 | 0.3320 | 508.93 | -39.33 | 0.5955 | -174.93 | 0.8250 | -0.2635 |
| 2 | 38.20 | -28.40 | 0.4560 | 9.76 | -28.18 | 0.5248 | 28.44 | -0.2167 | -0.0688 |
| 3 | 250.40 | -31.80 | 0.4580 | -136.59 | -30.02 | 0.4422 | 386.99 | -1.78 | 0.0158 |
| 4 | 56.85 | -31.90 | 0.3340 | 102.95 | -33.39 | 0.3348 | -46.10 | 1.49 | -0.0008 |
| 5 | 496.10 | -38.80 | 0.4050 | 289.09 | -38.54 | 0.3705 | 207.01 | -0.2583 | 0.0345 |
| 6 | 218.00 | -32.70 | 0.4600 | 334.36 | -34.31 | 0.5290 | -116.36 | 1.61 | -0.0690 |
| 7 | 73.50 | -22.90 | 0.3370 | 214.35 | -17.96 | 0.3693 | -140.85 | -4.94 | -0.0323 |
| 8 | 76.00 | -18.90 | 0.4860 | 269.16 | -20.58 | 0.4717 | -193.16 | 1.68 | 0.0143 |
| 9 | 497.00 | -32.60 | 0.4780 | 415.86 | -37.63 | 0.4823 | 81.14 | 5.03 | -0.0043 |
| 10 | 254.80 | -32.70 | 0.5000 | 176.44 | -36.01 | 0.4772 | 78.36 | 3.31 | 0.0228 |
| 11 | 931.70 | -28.60 | 0.7500 | 813.41 | -33.33 | 0.6385 | 118.29 | 4.73 | 0.1115 |
| 12 | 200.30 | -24.90 | 0.5790 | 288.73 | -19.66 | 0.4425 | -88.43 | -5.24 | 0.1365 |
| 13 | 62.50 | -45.60 | 0.3590 | 131.17 | -40.24 | 0.3187 | -68.67 | -5.36 | 0.0403 |
| 14 | 214.20 | -23.40 | 0.3920 | 268.26 | -24.87 | 0.5495 | -54.06 | 1.47 | -0.1575 |
| 15 | 317.60 | -27.60 | 0.3070 | 280.46 | -27.40 | 0.3488 | 37.14 | -0.2000 | -0.0418 |
| 16 | 1662.00 | -10.50 | 0.4000 | 1083.75 | -13.67 | 0.5345 | 578.25 | 3.17 | -0.1345 |
| 17 | 497.00 | -32.90 | 0.5710 | 196.01 | -35.09 | 0.4480 | 300.99 | 2.19 | 0.1230 |
| 18 | 224.00 | -29.30 | 0.3660 | 196.91 | -30.80 | 0.3702 | 27.09 | 1.50 | -0.0042 |
| 19 | 845.00 | -25.90 | 0.7650 | 804.78 | -22.19 | 0.6168 | 40.22 | -3.71 | 0.1482 |
| 20 | 344.00 | -16.70 | 0.7370 | 445.76 | -18.88 | 0.5635 | -101.76 | 2.18 | 0.1735 |
| 21 | 270.80 | -26.70 | 0.3240 | 501.40 | -24.81 | 0.4132 | -230.60 | -1.89 | -0.0892 |
| 22 | 265.00 | -23.80 | 0.3920 | 678.01 | -23.11 | 0.5050 | -413.01 | -0.6917 | -0.1130 |
| 23 | 786.00 | -22.10 | 0.7670 | 879.16 | -23.89 | 0.6900 | -93.16 | 1.79 | 0.0770 |
| 24 | 439.30 | -51.20 | 0.4870 | 602.12 | -44.53 | 0.4055 | -162.82 | -6.67 | 0.0815 |

**The Polydispersity Index (PDI)**

It is a key parameter used to describe the size distribution of nanoparticles. It ranges from 0 to 1, where values closer to 0 indicate a monodisperse system with uniform particle sizes, and values closer to 1 suggest a polydisperse system with a wide range of particle sizes. A PDI value below 0.3 is often considered acceptable for drug delivery applications. The concentration of Poloxamer 407 not only influences the average particle size but also affects the PDI, which reflects the uniformity of particle sizes. Higher concentrations of Poloxamer 407 typically result in a lower PDI, indicating a more monodisperse system with a narrower size distribution. This is because increased surfactant concentration promotes more consistent nanoparticle formation and stabilization, leading to particles of similar size [44].

**Rationale for the selection of excipients and their proportions and their linkage with observed results**

The selection and proportion of excipients in the formulation of MBSLNs were determined by their physicochemical compatibility with the APIs, their function in enhancing the formation and stability of nanoparticles, and supporting data from scientific literature.

***Stearic Acid (Lipid Core)***

Because of its proven ability to create stable SLNs, room-temperature solidification characteristics, and biocompatibility, stearic acid was selected as the primary lipid. It provides a hydrophobic environment that is favorable for the encapsulation of metformin and berberine, thereby enhancing the stability of the nanoparticles and prolonging the release of the drugs. The concentration of stearic acid significantly influenced particle size and zeta potential; higher concentrations created a denser lipid matrix, resulting in smaller particles and a more negative zeta potential due to the increased exposure of free carboxyl groups on the particle surface [45]. A rise in negative zeta potential amplifies particle repulsion, thereby reducing

aggregation and resulting in a diminished PDI and improved stability. Furthermore, an increased concentration of stearic acid enhances lipid compactness and reduces surface curvature, resulting in smaller globule sizes due to its influence on solid-state lipid crystallinity [46].

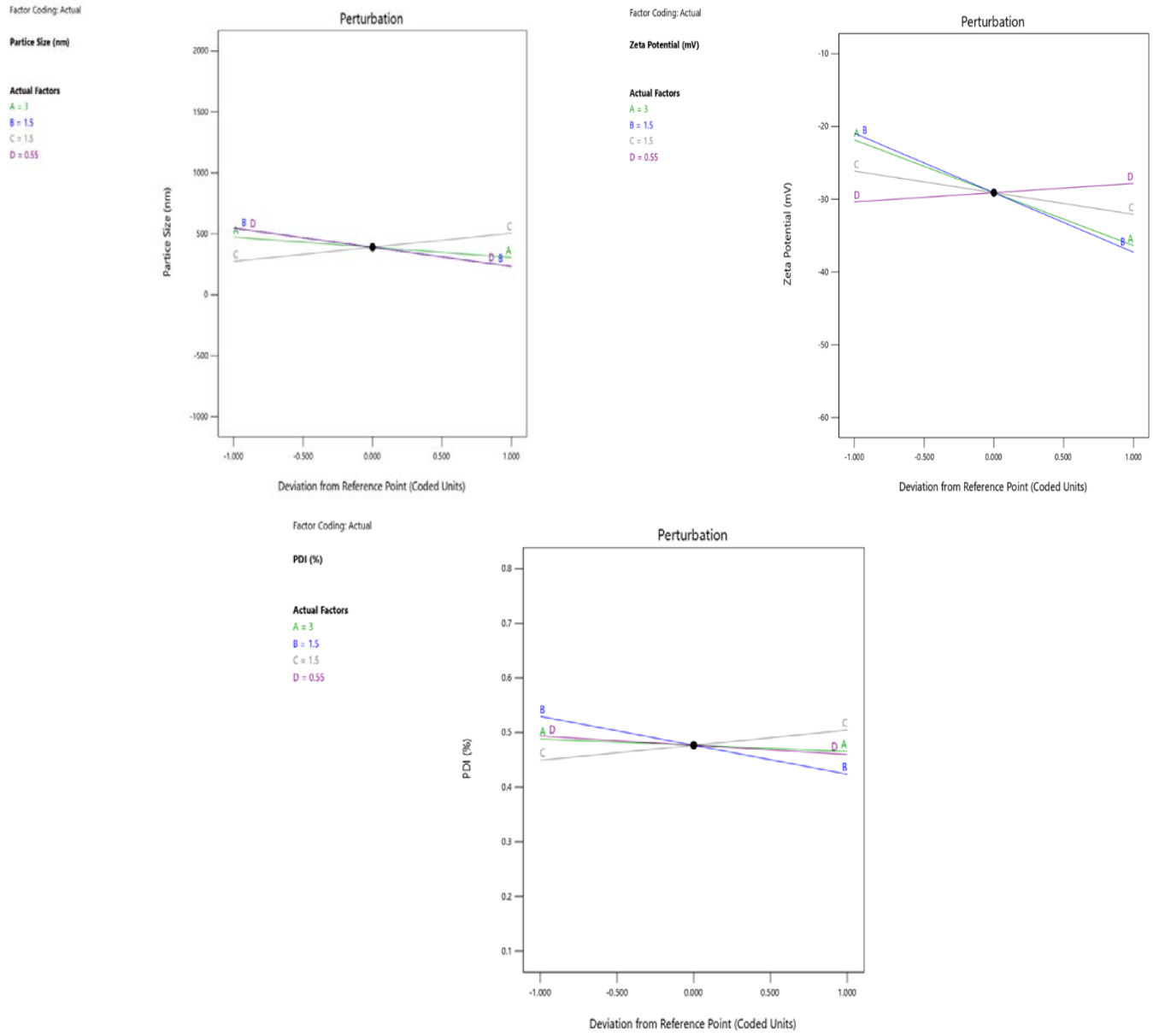


**Figure 1: The perturbation graph of (a) particle size, (b) zeta potential, (c) Polydispersity Index, showing the effect of factor A–Stearic acid, B–polysorbate 80, C- Poloxamer 407, and D – sesame oil concentration.**

***Polysorbate 80(Tween 80)***

A non-ionic surfactant called Polysorbate 80 was used to enhance the stability of the nanoparticles by reducing the interfacial tension between the lipid and aqueous phases. Its amphiphilic structure reduces particle agglomeration by facilitating effective adsorption onto the lipid core. To provide enough surface covering and prevent micelle formation, which could jeopardize particle homogeneity & increase polydispersity, a concentration range of 1-2 mL was chosen. By lowering interfacial tension, Tween 80 encourages emulsification between the lipid and aqueous phases. Because it is amphiphilic, it can adsorb at the oil-water interface, stabilizing tiny droplets while homogenizing [47]. Excessive use, however, may result in micelle production or competition for space at the

interface, raising the PDI or causing droplet coalescence. The observed drop in zeta potential at concentration Z is likely due to the sheltering of surface charges by its non-ionic surfactant chains.

***Poloxamer 407 (Stabilizer/Surfactant)***

By creating a hydrated shell around the nanoparticles, Poloxamer 407 was added to improve steric stabilization and system stability. To reduce particle aggregation and lower the PDI, this steric barrier is crucial. Poloxamer 407 stabilizes nanoparticles by providing a steric hindrance at their surface. With increased concentration, the polymer distributes more uniformly, limiting aggregation and resulting in a reduced PDI and a more uniform particle size distribution [48]. However, at elevated levels, the extended polymeric corona may produce a modest increase in particle size due to the thickened surface layer around each nanoparticle. Based on earlier research showing ideal nanoparticle homogeneity and improved drug encapsulation at these concentrations, a concentration range of 1-2 g was chosen.

***Sesame Oil (Co-lipid/Permeation Enhancer)***

Due to its antioxidant and neuroprotective properties, sesame oil was selected for its efficacy as a natural permeation enhancer, particularly for brain-targeted delivery [49]. Rich in unsaturated fatty acids and antioxidants like sesamol and sesamin, sesame oil acts as a co-lipid to improve the lipid matrix's fluidity and affect the dynamics of drug release. When used at low doses, it efficiently incorporates into the lipid framework without reducing nanoparticle stiffness. Notably, its presence has been linked to a higher zeta potential, likely due to surface contacts that limit charge masking and enhance electrostatic repulsion. It also modifies the kinetics of drug release and increases the flexibility of the lipid matrix. Because of the modest conc. range (0.1–1mL), the flexibility of the nanoparticles was increased without sacrificing their structural integrity.

Optimal quantities of stearic acid (4.84%), polysorbate 80 (1.50%), poloxamer 407 (1.00%), and sesame oil (0.31%) were determined using the Box-Behnken Design (BBD) in conjunction with response surface methodology (RSM). This strategic method facilitated the development of nanoparticles with optimal particle size, zeta potential, and PDI designed explicitly for effective brain-targeted delivery. The distinct physicochemical properties of berberine and metformin affect their ability to cross the blood-brain barrier. Encapsulating these chemicals in SLNs with surfactants has shown potential for improving their traversal across the blood–brain barrier (BBB). Metformin, known for its positive charge and high hydrophilicity, displays poor passive diffusion over the BBB. Nonetheless, it can pass through the brain via organic cation transporters (OCTs), primarily OCT1, which is present on the endothelial cells of the brain. Pathological conditions, such as inflammation or hypoxia, may further promote this transfer. Moreover, metformin's stimulation of AMP-activated protein kinase (AMPK) in endothelial cells has been linked to variations in tight junction integrity, which may influence BBB permeability [50]. Berberine, which is an isoquinoline alkaloid with low water solubility and limited oral bioavailability, is assumed to cross the BBB mostly through passive diffusion and perhaps via carrier-mediated routes. However, its specific transport mechanisms are still being understood. In addition to its transport capacity, berberine contributes to BBB protection by mitigating oxidative stress, inhibiting matrix metalloproteinase-9 (MMP-9) activity, and minimizing inflammatory cytokine levels—factors that collectively facilitate its delivery to the brain [51].To improve BBB penetration, SLNs must contain surfactants like polysorbate 80 and poloxamer 407. For example, polysorbate 80 can adsorb apolipoprotein E from plasma onto the surface of the nanoparticle, allowing receptor-mediated transcytosis through the low-density lipoprotein (LDL) receptors of brain capillary endothelial cells [52]. Similarly, poloxamer 407 can prolong nanoparticle residence at the blood-brain barrier and enhance drug accumulation in the central nervous system by blocking efflux transporters such as P-glycoprotein (P-gp). Surfactant-mediated receptor targeting, efflux modulation, drug-specific transport pathways, and the nanoformulation's capacity to protect and sustain release all work together to significantly increase the probability that therapeutic concentrations of berberine and metformin will reach the brain. The long-term use of solid lipid nanocarriers (SLNs) is typically considered safe, primarily due to their composition using scientifically approved excipients. For instance, when mice were repeatedly administered SLNs composed of triestearin or natural wax, moderate localized inflammation and absorption were observed in the adipose tissues. Still, no systemic toxicity, weight changes, or significant biochemical abnormalities occurred. However, despite these promising findings, vigilance remains needed. Some studies have demonstrated hepatic oxidative stress associated with

SLNs, as evidenced by lipid peroxidation and decreased antioxidant activity in certain animal models. Thus, while SLNs have a promising preclinical safety profile, their continued use should be followed by cautious surveillance for mild tissue-specific effects, especially those involving inflammatory or oxidative responses.

***Optimization of formulation using graphical optimization***

Optimization of SLNs was performed to determine the levels of factors A to D, which resulted in y1 (particle size) within the 10-200nm range, y2 (zeta potential) in the ±30 mV range, and y3 (PDI) in the 0-1 range. It was discovered that the values of the observed yi-y3 responses closely matched the expected values, demonstrating the reliability of the optimization process. The DOE software's overlay plot of graphical optimization to obtain responses in the desired range is shown in Figure 2. Finally, the optimized concentrations of the variable factors were stearic acid (4.84%), Polysorbate 80 (1.50%), Poloxamer 407 (1%), and sesame oil (0.31%); Table 7 shows the final optimized formulation concentrations.

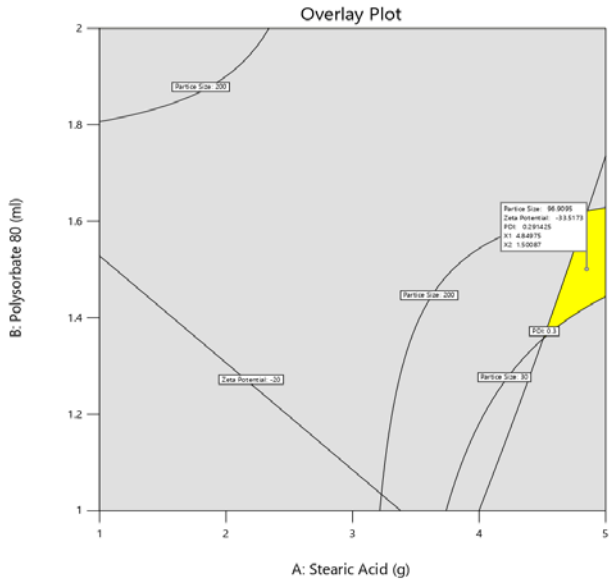


**Figure 2: Represents the overlay plot of particle size, Zeta Potential, and PDI for the optimization parameter suggested by the DOE software for the response in the desired range.**

**Optimization validation**

The optimum solid lipid nanoparticle (SLN) formulation was determined based on the parameters of achieving the lowest particle size ($Y_1$), maximum magnitude of negative zeta potential ($Y_2$), and low PDI $Y_3$) lying in the experimental range. The following responses were predicted by numerical optimization for an ideal batch: Particle size = 102.95 nm, Zeta potential = –33.39 mV, PDI = 0.3348. A fresh batch was prepared with the expected formulation composition to confirm the reliability of the optimization. The experimentally obtained parameters were a particle size of 56.85 nm, a PDI of 0.3340, and a Zeta potential of –31.90 mV. The variations between predicted and experimental values equate to residuals of –46.10 nm for particle size, 1.49 mV for zeta potential, and –0.0008 for PDI, suggesting a close agreement. The optimized formulation revealed a particle size well within the nanoscale range, a sufficiently strong negative zeta potential to provide electrostatic stabilization, and a low PDI indicating uniform particle dispersion. The optimization model's validity and robustness are confirmed by the close match between actual and predicted values, demonstrating the effectiveness and reproducibility of the experimental design technique used.

**Table 7: Details of the final optimized formulation**

| S. No | Ingredients | Quantity |
|---|---|---|
| 1 | Stearic acid | 4.84 |
| 2 | Polysorbate 80 | 1.50 |
| 3 | Poloxamer 407 | 1 |
| 4 | Sesame oil | 0.31 |
| 5 | Distilled water | Quantity sufficient for 50 g |

**Entrapment efficiency**

The effectiveness of the lipid matrix in encapsulating the drug molecules was evaluated by measuring the entrapment efficiency (EE) of the prepared SLNs. For Metformin HCl-loaded SLNs, the EE was assessed at 94 ± 1%, showing near-complete incorporation of the drug into the lipid core. This high amount of encapsulation is primarily due to metformin's hydrophilic characteristics and its remarkable affinity for the lipid phase during nanoparticle production, which limits drug loss during the manufacturing process. In comparison, the Berberine chloride-loaded SLNs displayed an EE of 63 ± 2%, which, although moderate, nonetheless represents a satisfactory drug entrapment. The significantly lower EE may be due to the molecular structure and physicochemical properties of berberine chloride, particularly its decreased compatibility with the lipid phase, which can contribute to significant drug leakage during the solidification stage.

**In Vitro release study**

A drug exerts its therapeutic effects only when it is released from its dosage form and disperses into the biological environment.

The release profiles of metformin and berberine were studied, and a summary of the data is shown in Figure 3.

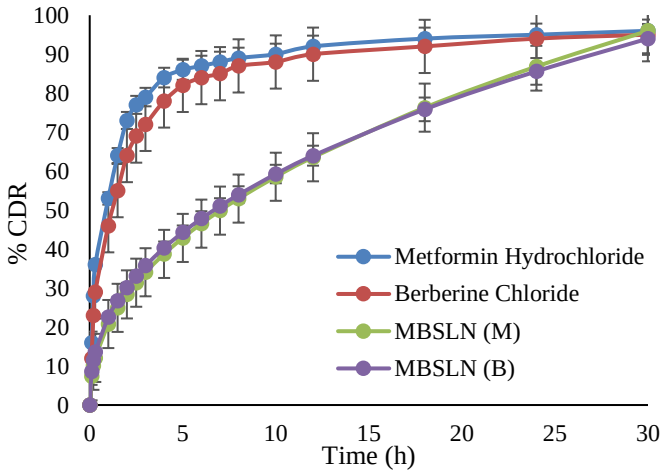


**Figure 3: In vitro drug release profile for Metformin, Berberine, and MBSLNs**

Over 24 hours, the cumulative drug release from the improved SLN formulations of berberine and metformin was 73 ± 2% and 76 ± 1%, respectively. Both of the drugs displayed an initial burst release, followed by a continuous and progressive release over the 24-hour duration. This release profile aligns with patterns observed in previous investigations [ref]. The strong burst release, notably in the case of berberine chloride, resulted in nearly 30% of the medication being released within the first 2 hours. This occurrence is attributed to the existence of free or loosely bound drug molecules, which were more abundant in berberine due to its lower EE compared to metformin, hence leading to a higher concentration of unencapsulated drug. With the help of the DDSolver Excel add-in, a model-dependent method was used to assess the release kinetics mechanism. The ideal release model was identified based on major statistical variables, including the adjusted coefficient of determination ($R^2$_adj), MSC, and AIC. A comparative review of these indicators is provided in Table 8. Among the investigated models, the Korsmeyer–Peppas model emerged as the most suitable for defining the drug release behavior across all formulations, displaying the greatest $R^2$_adj, the most favorable MSC, and the lowest AI values compared to other kinetic models. Table 8 provides a summary of the release exponent (n) values obtained using the Korsmeyer–Peppas model. Across all formulations, the n values were determined to be below 0.45, showing that the drug release adhered to Fickian diffusion dynamics. This suggests that the release mechanism was primarily driven by the diffusion of drug molecules from the nanoparticles into the surrounding medium.

**Table 8: Kinetics and mechanism of release parameters for solid lipid nanocarrier formulations**

| | R2 _adj. | n | AIC | MSC | R2 _adj. | n | AIC | MSC |
|---|---|---|---|---|---|---|---|---|
| **Zero order** | 0.8997 | - | -90.41 | 2.360 | 0.8861 | - | -89.46 | 2.233 |
| **First order** | 0.9782 | - | -117.91 | 3.888 | 0.9839 | - | -124.65 | 4.188 |
| **Higuchi** | 0.9987 | - | -168.34 | 6.689 | 0.9965 | - | -152.37 | 5.728 |
| **Korsmeyer-Peppas** | 0.9995 | 0.4500 | -288.64 | 17.217 | 0.9975 | 0.4199 | -282.13 | 16.731 |

***Neuroprotective studies***

Animals were induced with a combination of toxins to induce T2DM and later dementia, and significant changes in the reduction of neurodegeneration were observed from the beginning till the treatment was given. A 90-day sample was taken for the histopathological, biochemical, and behavioral evaluation to observe the significant changes. The oxidative stress and hyperglycemic effects have been significantly reduced compared to those of normal controls.

***EVALUATION OF BEHAVIORAL PARAMETERS FOR THERAPEUTIC POTENTIAL OF MBSLNPS***

***MWM and Y maze test***

A battery of behavioral tests, including the MWM and Y-maze, was conducted to assess the cognitive and neurobehavioral effects of MBSLNPs in this T2DM-induced AD animal model. In the MWM test, rats in the disease control group exhibited marked spatial memory deficits, as evidenced by a significant reduction in time spent in the target quadrant and an increase in latency time compared to the normal control. Treatment with MBSLNPs resulted in a significant dose-dependent improvement in the memory of Wistar rats. Total time to swim quadrant increased to 7.0 sec, 11.1sec,14.5sec, 16sec to 18.5 seconds & latency time decreased from 80 seconds to 60 seconds with each successive dose (Figure 3A, B). In the Y-maze test, the disease control group demonstrated impaired working memory, characterized by reduced spontaneous alternation performance and increased escape latency, compared to the normal control. MBSLNPs significantly improved the spontaneous alternation performance (10.87–28.42%) and escape latency (7.98–20.30 s) in a dose-dependent manner (Figure 3C, D)

***Histopathological analysis***

Histopathological examination was performed on the brain samples from control, toxin-treated, and SLN-treated groups on the 90th day. As shown in Figure 4, the brain exhibits a normal architecture. Histopathological examination of the diseased sample showed significant deterioration in brain structure, showing gliosis & demyelination, necrosis, apoptotic neurons, astroglia degeneration, and the presence of amyloid plaques and NFTs. The MBSLN-treated samples showed reduced glial edema, preserved neuronal architecture, and reduced neuroinflammation**.**

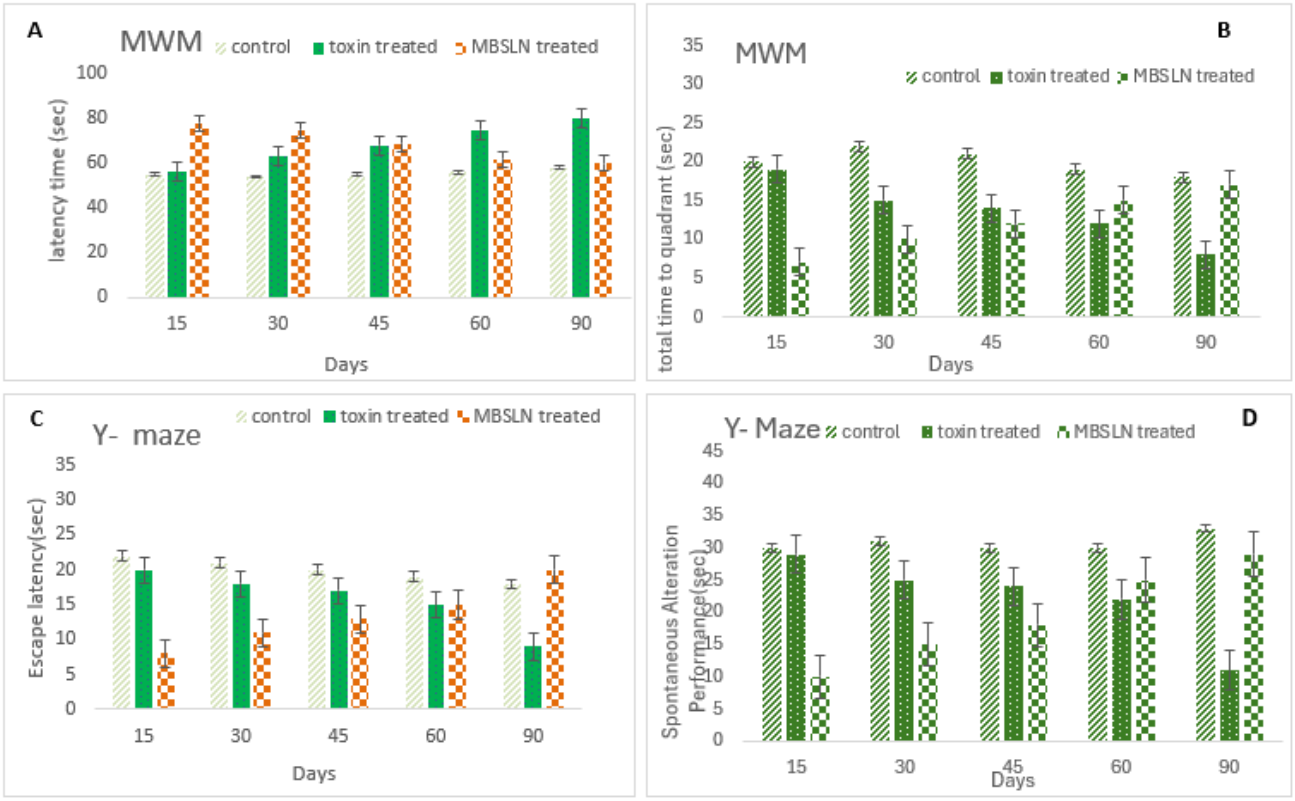


**Figure 3: Assessment of cognitive function in rats across multiple behavioral tests, including the Morris water maze (MWM) and Y-Maze. All values are represented in mean ± SD. (*) showed a significant difference (p <0.05) as compared with the normal control group and ($) showed a significant difference (p <0.05) as compared with the disease control group.**

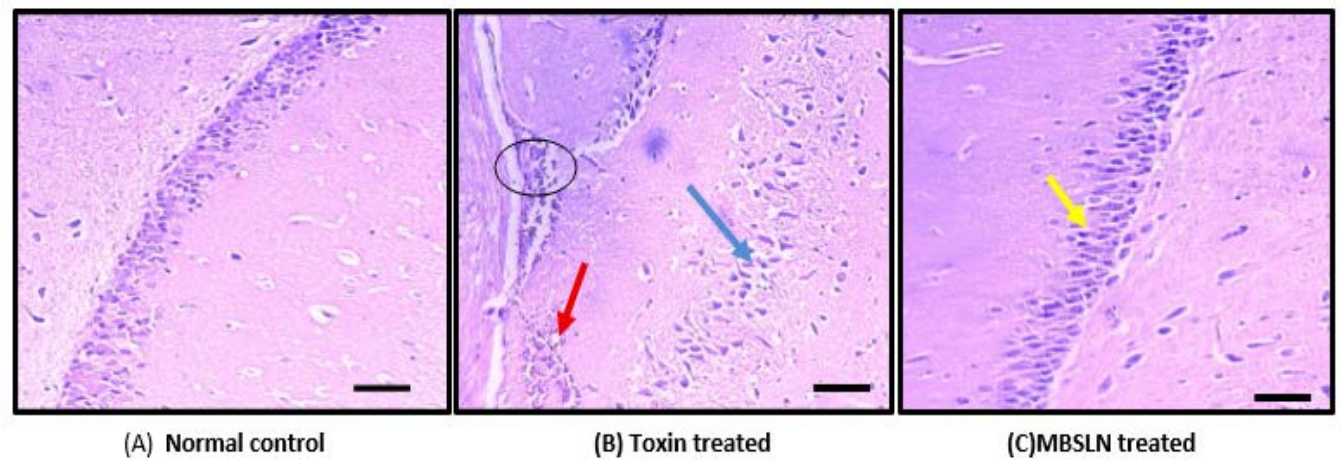


**Figure 4: Photomicrographs of histopathological changes in brain tissue sections (sacrificed on the 90th day) of (A) control showing cells within normal limit (B) toxin treated showing hippocampal degeneration (blue arrow), glial edema (black circle) and inflammation (red arrow) (C) MBSLN treated samples showing reduced inflammation (yellow arrow) and cells regaining normal limits. Imaging was performed using Motic BA310 microscope at 100× magnification (scale bar = 100 µm)**

***Biochemical analysis***

1. **Catalase:** The antioxidant potential of the blood serum catalase enzymes was evaluated using the catalase test. The serum of the treatment subjects displayed an increased spike in catalase activity compared to the control subjects (Figure 5A). On the 15th day, the catalase activity recorded was 9.75 nmole/min/mg, and it eventually increased to 38.65 nmole/min/mg on the 90th day of SLN treatment. An increase in catalase activity can be indicative of increased inflammatory response in the blood.

**2. AChE activity:** AChE levels were measured in the brain tissue of the control and the SLN-treated subjects. In the treated subjects, during the 1st 15 days, AChE levels were noted as 0.0132 µmoles/min/mg ($p < 0.0001$ **), but they significantly rose to 0.0275 µmoles/min/mg by the 90$^{th}$ day of SLN treatment. During the progression of the disease, it was observed that AChE levels declined compared to the control group, while they increased with simultaneous SLN treatment (Figure 5B). An increase in AChE levels is suggestive of improved neuronal signaling.

**3. Glucose estimation:** In addition to being a fuel, glucose is an important attribute, since its presence can help assess how well cells absorb glucose & thus indicate insulin resistance. Neurons absorb energy from glucose to survive and function. Serum glucose levels were also measured in control & SLN trea- ted subjects in diseased condition, the blood glucose levels spiked to 275mg/gl. With the simultaneous SLN treatment doses, serum glucose levels seemed to decrease progressively (Figure 5C).

**4. Lipid peroxidation/MDA level estimation**: Serum samples were subjected to the lipid peroxidation assay to measure the body's levels of antioxidants and inflammation. The level of inflammation was directly proportional to the MDA formed in the sample. As seen in Figure 4D, the levels of MDA declined significantly & gradually in SLN-treated subjects ($p < 0.0001$). Graphical representation of significant changes in the: a) Catalase activity (n mole/$H_2O_2$ consumed/min/mg protein), b) AChE activity (µ mole/min/mg protein) c) glucose levels(mg/dl) d) MD A level (nmole/min/mg protein) in wistar rat serum (Figure. 5D).

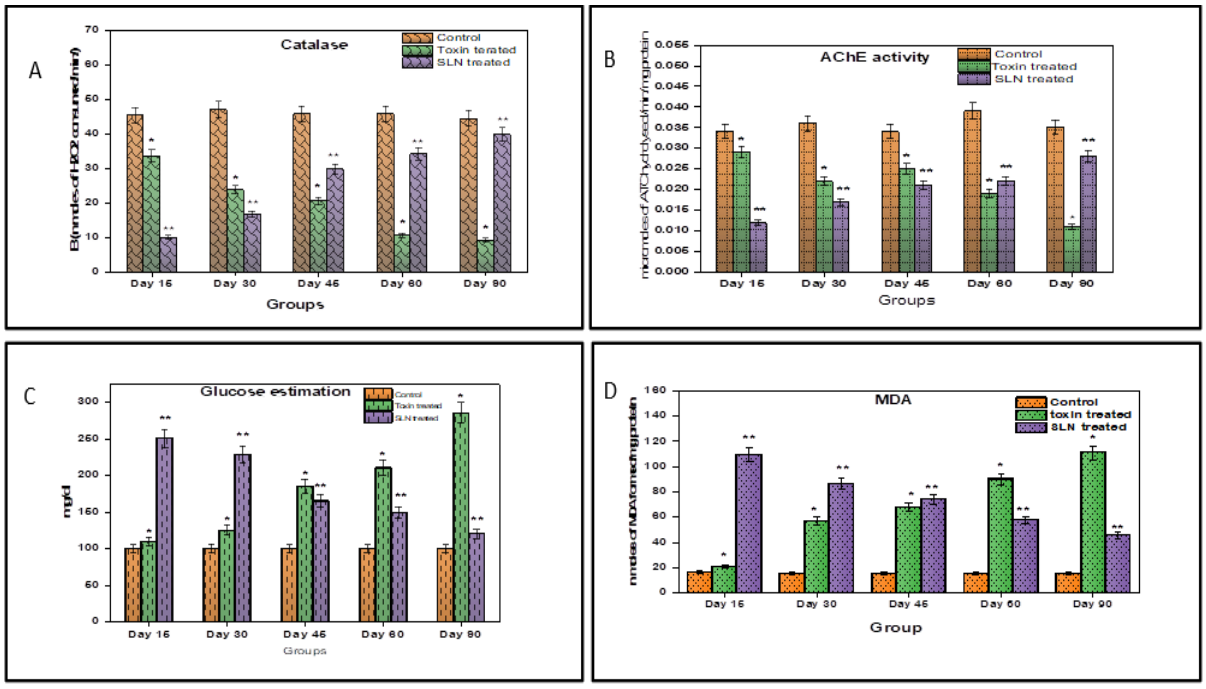


**Figure 5: Graphical representation of significant changes in the: a) Catalase activity (n mole/$H_2O_2$ consumed/min/mg protein), b) Acetylcholine esterase (AChE) activity (µ mole/min/mg protein) c) glucose levels(mg/dl) d) MDA level (nmole/min/mg protein) in Wistar rat serum**

***CONCLUSION***

The solid lipid nanocarriers loaded with metformin and berberine formulation are a potentially effective approach to treating a type of neurodegenerative condition closely associated with brain insulin resistance. Improved stability, targeted administration, controlled release of drugs, and increased

bioavailability are just a few benefits of using solid lipid nanocarriers, all of which are essential for the management of neurological dysfunctions. Metformin enhances insulin sensitivity and glucose management, while berberine exhibits antioxidant and anti-inflammatory properties. Together, these two medications have complementary therapeutic effects. The nanocarrier system further improves the therapeutic efficacy of these drugs by optimizing their brain absorption and minimizing systemic side effects. Indeed, the combination of these medications in lipid-based nanocarriers has synergistic effects that have the potential to significantly enhance Type 3 diabetes treatment options and provide more effective control of the disease's neurodegenerative processes. To thoroughly investigate the potential advantages and safety of these nanocarriers in human applications, further investigation and clinical trials are needed.

The qualified MBSLNs were affected by the examined independent parameters of stearic acid, polysorbate 80, Poloxamer 407, and sesame oil concentrations. The prepared MBSLNs with a high content of stearic acid and poloxamer 407 exhibited a significant effect on particle size and zeta potential. The utilization of MBSLNs has emerged as a remarkably effective strategy for enhancing the biological activity of Metformin and berberine in the treatment of Type 3 Diabetes.

While the BBD optimization produced accurate predictions, its fundamental limitations may hinder extrapolation beyond the established formulation parameters, particularly in scale-up situations or differing storage circumstances. The in vivo outcomes, indicating neuroprotection, had been primarily limited to biochemical and glucose-level evaluations, lacking thorough behavioral or cognitive examinations to validate functional outcomes. The lack of comprehensive histological analysis of brain tissues restricts understanding of cellular-level neuroprotection. Such shortcomings underscore the need for extensive experimental validation to enhance translational confidence in the optimized MBSLN formulation for addressing neurodegeneration associated with T2DM**.**

Future studies should explore the scalability of optimized MBSLNs through reproducible and cost-effective production methods, guaranteeing uniform particle size, stability, and drug encapsulation. The long-term safety must be assessed through GLP-compliant chronic toxicity studies involving numerous species, including biodistribution and neurobehavioral evaluations. Translational initiatives must focus on creating clinical-grade formulations, engaging with regulatory bodies, and conducting early-phase clinical trials to assess neuroprotective biomarkers, pharmacokinetics, and safety in patients with T2DM and AD. To establish MBSLNs as a successful treatment approach for diabetes-related neurodegeneration, further research is needed into BBB penetration mechanisms, biomarker validation, and formulation stability.

***FINANCIAL ASSISTANCE***
NIL

***CONFLICT OF INTEREST***
The authors declare no conflict of interest.

***AUTHOR CONTRIBUTION***
Ashish Kumar and Ravina Yadav contributed to the design of the study to ensure a robust and effective review framework. Ravina Yadav played a critical role in writing the original draft. Deepshikha Pande Katare and Ruchi Jakhmola Mani conceptualized and did the formal analysis. Arun Kumar, Ravina Yadav, and Ashish Kumar contributed to the methodology and software analysis part. Arun Kumar and Deepshikha Pande Katare drafted and edited it, contributing to its overall coherence and quality. All the authors read and approved the final manuscript, confirming their agreement with the content and conclusions presented.

***REFERENCES***
[1] Butterfield DA, Di Domenico F, Barone E. Elevated risk of type 2 diabetes for development of Alzheimer disease: a key role for oxidative stress in brain. *Biochimica et Biophysica Acta (BBA)-Molecular Basis of Disease*, **1842(9),** 1693-706 (2014) https://doi.org/10.1016/j.bbadis.2014.06.010.

[2] Liu S, Liu T, Li J, Hong J, Moosavi-Movahedi AA, Wei J. Type 2 Diabetes Mellitus Exacerbates Pathological Processes of Parkinson's Disease: Insights from Signaling Pathways Mediated by Insulin Receptors. *Neurosci Bull*, **41(4),** 676-690 (2025) https://doi.org/10.1007/s12264-024-01342-8.

[3] Dave BP, Shah YB, Maheshwari KG, Mansuri KA, Prajapati BS, Postwala HI, Chorawala MR. Pathophysiological aspects and therapeutic armamentarium of Alzheimer's disease: recent trends and future development. *Cellular and Molecular Neurobiology*, **43(8),** 3847-84 (2023) https://doi.org/10.1007/s10571-023-01408-7.

[4] Kciuk M, Kruczkowska W, Gałęziewska J, Wanke K, Kałuzińska-Kołat Ż, Aleksandrowicz M, Kontek R. Alzheimer's Disease as Type 3 Diabetes: Understanding the Link and Implications. *International Journal of Molecular Science*s, **25(22),** 11955 (2024) https://doi.org/10.3390/ijms252211955.

[5] Zhao WQ, Townsend M. Insulin resistance and amyloidogenesis as common molecular foundation for type 2 diabetes and Alzheimer's disease. *Biochimica et Biophysica Acta (BBA)-Molecular Basis of Disease*, **1792(5)**, 482-96 (2009) https://doi.org/10.1016/j.bbadis.2008.10.014.

[6] Zhao WQ, Chen H, Quon MJ, Alkon DL. Insulin and the insulin receptor in experimental models of learning and memory. *Eur J Pharmacol*, **490(1-3)**, 71-81 (2004) https://doi.org/10.1016/j.ejphar.2004.02.045.

[7] Abdalla MM. Insulin resistance as the molecular link between diabetes and Alzheimer's disease. *World Journal of Diabetes*, **15(7)**, 1430 (2024) https://doi.org/10.4239/wjd.v15.i7.1430.

[8] Affuso F, Micillo F, Fazio S. Insulin Resistance, a Risk Factor for Alzheimer's Disease: Pathological Mechanisms and a New Proposal for a Preventive Therapeutic Approach. *Biomedicines*, **12(8)**, 1888 (2024) https://doi.org/10.3390/biomedicines12081888.

[9] Lv Z, Guo Y. Metformin and Its Benefits for Various Diseases. *Front Endocrinol* (*Lausanne)*, **11**, 191 (2020) https://doi.org/10.3389/fendo.2020.00191.

[10] Triggle CR, Mohammed I, Bshesh K, Marei I, Ye K, Ding H, MacDonald R, Hollenberg MD, Hill MA. Metformin: Is it a drug for all reasons and diseases? *Metabolism*, **133**, 155223 (2022) https://doi.org/10.1016/j.metabol.2022.155223.

[11] Ekor M. The growing use of herbal medicines: issues relating to adverse reactions and challenges in monitoring safety. *Front Pharmacol*, **4**, 177 (2014) https://doi.org/10.3389/fphar.2013.00177.

[12] Liu D, Meng X, Wu D, Qiu Z, Luo H. A Natural Isoquinoline Alkaloid with Antitumor Activity: Studies of the Biological Activities of Berberine. *Front Pharmacol*, **10**, 9 **(**2019) https://doi.org/10.3389/fphar.2019.00009.

[13] Tian E, Sharma G, Dai C. Neuroprotective Properties of Berberine: Molecular Mechanisms and Clinical Implications. *Antioxidants (Basel*), **12(10),** 1883 (2023) https://doi.org/10.3390/antiox12101883.

[14] Wang H, Zhu C, Ying Y, Luo L, Huang D, Luo Z. Metformin and berberine, two versatile drugs in treatment of common metabolic diseases. *Oncotarget*, **9(11),** 10135-10146 (2017) https://doi.org/10.18632/oncotarget.20807.

[15] Lyu Y, Li D, Yuan X, Li Z, Zhang J, Ming X, Shaw PC, Zhang C, Kong AP, Zuo Z. Effects of combination treatment with metformin and berberine on hypoglycemic activity and gut microbiota modulation in db/db mice. *Phytomedicine*, **101,** 154099 (2022) https://doi.org/10.1016/j.phymed.2022.154099.

[16] Hao Y, Li J, Yue S, Wang S, Hu S, Li B. Neuroprotective effect and possible mechanisms of berberine in diabetes-related cognitive impairment: a systematic review and meta-analysis of animal studies. *Frontiers in Pharmacology*, **13,** 917375 (2022) https://doi.org/10.3389/fphar.2022.917375.

[17] Kodi T, Praveen S, Paka SK, Sankhe R, Gopinathan A, Krishnadas N, Kishore A. Neuroprotective Effects of Metformin and Berberine in Lipopolysaccharide-Induced Sickness-Like Behaviour in Mice. *Adv Pharmacol Pharm Sci*., **2024,** 8599268 (2024) https://doi.org/10.1155/2024/8599268.

[18] Bukke SP, Venkatesh C, Bandenahalli Rajanna S, Saraswathi TS, Kusuma PK, Goruntla N, Balasuramanyam N, Munishamireddy S. Solid lipid nanocarriers for drug delivery: design innovations and characterization strategies—a comprehensive review. *Discover applied sciences*, **6(6),** 279 **(**2024) https://doi.org/10.1007/s42452-024-05897-z.

[19] Al-Hazmi GA, Elsayed NH, Alnawmasi JS, Alomari KB, Alessa AH, Alshareef SA, El-Bindary AA. Elimination of Ni (II) from wastewater using metal-organic frameworks and activated algae encapsulated in chitosan/carboxymethyl cellulose hydrogel beads: Adsorption isotherm, kinetic, and optimizing via Box-Behnken design optimization. *International Journal of Biological Macromolecules*, **299,** 140019 (2025) https://doi.org/10.1016/j.ijbiomac.2025.140019.

[20] Baltz N, Scherließ R. Entrapment efficiency methodology for lipid nanoparticles–a literature review. *OpenNano*, 100251 (2025) https://doi.org/10.1016/j.onano.2025.100251.

[21] Baek JS, Cho CW. Surface modification of solid lipid nanoparticles for oral delivery of curcumin: Improvement of bioavailability through enhanced cellular uptake, and lymphatic uptake. *European Journal of Pharmaceutics and Biopharmaceutics*, 132-140 (2017**)** https://doi.org/10.1016/j.ejpb.2017.04.013.

[22] Kamarudin NB, Sharma S, Gupta A, Kee CG, Chik SMSBT, Gupta R. Statistical investigation of extraction parameters of keratin from chicken feather using Design-Expert. *3 Biotech*, **7**, 1–9 (2017) https://doi.org/10.1007/s13205-017-0767-9.

[23] Ferreira SC, Bruns RE, Ferreira HS, Matos GD, David JM, Brandão GC, da Silva EP, Portugal LA, Dos Reis PS, Souza AS, Dos Santos WN. Box-Behnken design: an alternative for the optimization of analytical methods. *Analytica chimica acta*, **597(2),** 179-86 (2017) https://doi.org/10.1016/j.aca.2007.07.011.

[24] Sopyan IY, Gozali DO, Kurniawansyah IS, Guntina RK. Design-expert software (DOE): An application tool for optimization in pharmaceutical preparations formulation. *International Journal of Applied Pharmaceutics*, **14(4),** 55-63 (2022) https://doi.org/10.22159/ijap.2022v14i4.45144.

[25] Maran JP, Manikandan S. Response surface modeling and optimization of process parameters for aqueous extraction of pigments from prickly pear (Opuntia ficus-indica) fruit**.** *Dyes and*

*Pigments*, **95(3),** 465-72 (2012) https://doi.org/10.1016/j.dyepig.2012.06.007.

[26] Jakhmola Mani R, Dogra N, Katare DP. The connection between chronic liver damage and sporadic Alzheimer's disease: evidence and insights from a rat model. *Brain Sciences*, **13(10),** 139 (2023) https://doi.org/10.3390/brainsci13101391.

[27] Knezovic A, Hosch M, Hamann CS, Popp S, Ortega G, Osmanovic-Barilar J, Grünblatt E, Monoranu C, Riederer P, Salkovic-Petrisic M, Schmitt-Böhrer A. Approaching therapy of Alzheimer's disease via the antidiabetic drug liraglutide—a study with streptozotocin intracerebroventricularly treated Wistar rats. *Journal of Neural Transmission*, 1-22 (2025) https://doi.org/10.1007/s00702-025-02979-z.

[28] Owumi S, Chimezie J, Salami MO, Ishaya JA, Onyemuwa CV, Nnamdi M, Owoeye O. Lutein and Zeaxanthin abated neurobehavioral, neurochemical and oxido-inflammatory derangement in rats intoxicated with Aflatoxin B1. *Toxicon*, **258,** 108345 (2025) https://doi.org/10.1016/j.toxicon.2025.108345.

[29] Sharma AK, Kumar A, Kumar S, Mukherjee S, Nagpal D, Nagaich U, Rajput SK. Preparation and therapeutic evolution of Ficus benjamina solid lipid nanoparticles against alcohol abuse/antabuse induced hepatotoxicity and cardio-renal injury. *RSC advance*, **7(57),** 35938-49 (2017) https://doi.org/10.1039/C7RA04866A.

[30] Prokić M, Borković-Mitić S, Krizmanić I, Gavrić J, Despotović S, Gavrilović B, Radovanović T, Pavlović S, Saičić Z. Comparative study of oxidative stress parameters and acetylcholinesterase activity in the liver of *Pelophylax esculentus* complex frogs. *Saudi J Biol Sci***, 24(1),** 51-58 (2017)

[31] https://doi.org/10.1016/j.sjbs.2015.09.003.

[32] Kumari N, Mittal A, Rana A, Sharma AK. Callistemon viminalis extracts: dual action on anxiety and neuroprotection via neuroinflammatory and serotonergic pathways. *Neuroscience and Behavioral Physiology*, **55(1),** 61-73 (2025) https://doi.org/10.1007/s11055-024-01748-x.

[33] Ellman, G.L.; Courtney, K.D.; Andres, V., Jr.; Featherstone, R.M. A new and rapid colorimetric determination of acetylcholinesterase activity. *Biochem. Pharmacol*, **7,** 88–95 (1961) https://doi.org/10.1016/0006-2952(61)90145-9.

[34] Chigurupati S, Alharbi NA, Sharma AK, Alhowail A, Vardharajula VR, Vijayabalan S, Das S, Kauser F, Amin E. Pharmacological and pharmacognostical valuation of Canna indica leaves extract by quantifying safety profile and neuroprotective potential. *Saudi journal of biological sciences*, **28(10),** 5579-84 (2021) https://doi.org/10.1016/j.sjbs.2021.05.072.

[35] Rani A, Sharma PB, Bhatia S, Sharma AK. Comprehensive study on pharmacognostic, pharmacological, and toxicological features of Ficus racemosa in Alzheimer's disease using GC–MS and molecular docking analyses. *Toxicology Research*, **13(4),** tfae098 (2024) https://doi.org/10.1093/toxres/tfae098.

[36] Basak, A. Development of rapid and inexpensive plasma glucose estimation by two-point kinetic method based on glucose oxidase-peroxidase enzymes. *Indian J. Clin. Biochem*, **22,** 156–160 (2007) https://doi.org/10.1007/BF02912902.

[37] Wright, J.R.; Colby, H.D.; Miles, P.R. Cytosolic factors which affect microsomal lipid peroxidation in lung and liver. *Arch. Biochem. Biophys*, **206**, 296–304 (1981) https://doi.org/10.1016/0003-9861(81)90095-3.

[38] Kumar AS, Pandit VI, Nagaich UP. Preparation and evaluation of copper nanoparticles loaded with hydrogel for burns. *Int J App Pharm*, **13(2),**108-89 (2021) https://doi.org/10.22159/ijap.2021v13i2.40558.

[39] Johnson L, Gray DM, Niezabitowska E, McDonald TO. Multi-stimuli-responsive aggregation of nanoparticles driven by the manipulation of colloidal stability. *Nanosca*le, **13(17**), 7879-96 (2021) https://doi.org/10.1039/D1NR01190A.

[40] Öztürk K, Kaplan M, Çalış S. Effects of nanoparticle size, shape, and zeta potential on drug delivery. *International Journal of Pharmaceutics*, 124799 (2024) https://doi.org/10.1016/j.ijpharm.2024.124799.

[41] Usui S, Healy TW. Zeta potential of stearic acid monolayer at the air–aqueous solution interface. *Journal of colloid and interface science*, **250(2),** 371-8 (2002) https://doi.org/10.1006/jcis.2002.8340.

[42] Babayevska N, Przysiecka Ł, Iatsunskyi I, Nowaczyk G, Jarek M, Janiszewska E, Jurga S. ZnO size and shape effect on antibacterial activity and cytotoxicity profile. *Sci Rep*, **12(1),** 8148 (2022) https://doi.org/10.1038/s41598-022-12134-3.

[43] Bhatia S, Bhatia S. Nanoparticles types, classification, characterization, fabrication methods and drug delivery applications. *Natural polymer drug delivery systems: Nanoparticles, plants, and algae*, 33-93 (2016) https://doi.org/10.1007/978-3-319-41129-3_2.

[44] Rizvi SAA, Saleh AM. Applications of nanoparticle systems in drug delivery technology. *Saudi Pharm J*., **26(1),** 64-70 (2018) https://doi.org/10.1016/j.jsps.2017.10.012.

[45] Song T, Gao F, Guo S, Zhang Y, Li S, You H, Du Y. A review of the role and mechanism of surfactants in the morphology control of metal nanoparticles. *Nanoscale*, 13(7), 3895-910 (2021) https://doi.org/10.1039/D0NR07339C.

[46] Ignjatović J, Đuriš J, Cvijić S, Dobričić V, Montepietra A, Lombardi C, Ibrić S, Rossi A. Development of solid lipid microparticles by melt-emulsification/spray-drying processes as carriers for pulmonary drug delivery. *European Journal of Pharmaceutical Sciences*, **156,** 105588 (2021) https://doi.org/10.1016/j.ejps.2020.105588.

[47] Sambhakar S, Saharan R, Narwal S, Malik R, Gahlot V, Khalid A, Najmi A, Zoghebi K, Halawi MA, Albratty M, Mohan S.

Exploring LIPIDs for their potential to improves bioavailability of lipophilic drugs candidates: A review. *Saudi Pharmaceutical Journal*, **31(12),** 101870 (2023) https://doi.org/10.1016/j.jsps.2023.101870.

[48] Walia N, Zhang S, Wismer W, Chen L. A low energy approach to develop nanoemulsion by combining pea protein and Tween 80 and its application for vitamin D delivery. *Food Hydrocolloids for Health*, **2**, 0007 (2022) https://doi.org/10.1016/j.fhfh.2022.100078.

[49] Aldayel TS, Badran MM, Alomrani AH, AlFaris NA, Altamimi JZ, Alqahtani AS, Nasr FA, Ghaffar S, Orfali R. Optimization of cationic nanoparticles stabilized by Poloxamer 407 188: A potential approach for improving the biological activity of Aloe perryi. *Heliyon*, **9(12)** (2023) https://doi.org/10.1016/j.heliyon.2023.e22691.

[50] Abourehab MAS, Khames A, Genedy S, Mostafa S, Khaleel MA, Omar MM, El Sisi AM. Sesame Oil-Based Nanostructured Lipid Carriers of Nicergoline, Intranasal Delivery System for Brain Targeting of Synergistic Cerebrovascular Protection. *Pharmaceutics* ,**13(4),** 581 (2021) https://doi.org/10.3390/pharmaceutics13040581.

[51] Sharma S, Zhang Y, Akter KA, Nozohouri S, Archie SR, Patel D, Villalba H, Abbruscato T. Permeability of Metformin across an In Vitro Blood-Brain Barrier Model during Normoxia and Oxygen-Glucose Deprivation Conditions: Role of Organic Cation Transporters (Octs). *Pharmaceutics*, **15(5),** 1357 (2023) https://doi.org/10.3390/pharmaceutics15051357.

[52] Wu X, Liu X, Yang L, Wang Y. Berberine Protects against Neurological Impairments and Blood-Brain Barrier Injury in Mouse Model of Intracerebral Hemorrhage. *Neuroimmunomodulation*, **29(4),** 317-326 (2022) https://doi.org/10.1159/000520747.

[53] Kreuter J, Shamenkov D, Petrov V, Ramge P, Cychutek K, Koch-Brandt C, Alyautdin R. Apolipoprotein-mediated transport of nanoparticle-bound drugs across the blood-brain barrier. *J Drug Target*, **10(4),** 317-25 (2002) https://doi.org/10.1080/10611860290031877.